A Theoretical Study of Membrane Constraint in Polymer-Electrolyte Fuel Cells

Adam Z. Weber and John Newman
Dept. of Chemical Engineering, University of California, Berkeley, CA 94720

DOI 10.1002/aic.10230
Published online in Wiley InterScience (www.interscience.wiley.com).

A mathematical model is developed that examines the effect of having a constrained membrane in a fuel cell. During operation, a polymer-electrolyte fuel-cell membrane is prone to swell but is unable to do so by system design. This builds up a stress that affects transport in, and the properties of, the membrane. This report is the first to incorporate such effects into a macrohomogeneous model. Both the physical and mathematical effects are described. Results include the magnitude of constraint, the change in water content of the membrane attributed to constraint, and one-dimensional simulations showing the effect of constraint on the water balance of the fuel cell. The paper demonstrates the need for considering membrane constraint both in modeling and experimental studies of fuel cells. © 2004 American Institute of Chemical Engineers *AIChE J,* 50: 3215–3226, 2004

Introduction

Polymer-electrolyte (PE) or proton-exchange-membrane (PEM) fuel cells are on the verge of becoming one of the prominent technologies of the twenty-first century. Along with their attractiveness as efficient and clean energy producers, they may provide the energy structure of not only automotive but also residential applications. It is well known that current low-temperature ($\leq$80°C) PE fuel cells require inlet-gas humidification to operate efficiently. The reason is that the properties of the ionomer membrane, typically Nafion, are highly dependent on its water content.

Nafion is a copolymer of polytetrafluoroethylene and polysulfonyl fluoride vinyl ether. Like most other PEMs, it exhibits a high conductivity when fully hydrated, prodigious water uptake, and a tendency to swell. In an operating fuel cell, the fuel cell is constrained from swelling by the bipolar plates and the design of the system that ensures good contact among the various fuel-cell layers. Thus, although the membrane is prone to swell, it either is constrained or compresses the other layers in the fuel-cell sandwich. This is especially true for inlet regions where the membrane may be pinned by the bipolar plates, gaskets, seals, and so forth. Furthermore, it is known that a constrained membrane exhibits lower water content than that of an unconstrained one.[1,2] Mathematically, this behavior has never been examined and incorporated into a macroscopic model. The study reported herein seeks to do that by taking our previous membrane model[3] and incorporating the relevant stress equations. By examining the results of such a model, conclusions can be made on the effects and relative importance of having a constrained membrane. In addition, such a model can be adapted to predict fuel-cell failure and examine changes in the water balance arising from stress effects. The latter is important in designing an accurate water-management scheme.

Most previous macroscopic models treat swelling by assuming that the dimensions of the membrane remain constant (for examples, see Um et al.,[4] Nguyen and White,[5] and Bernardi and Verbrugge[6]). This thickness is often the thickness of the fully liquid-equilibrated membrane, but is sometimes another thickness such as the dry thickness. However, this treatment ignores how the dimensions change with water content and thus swelling, as well as any stress effects of having the membrane at the prescribed thickness. Another previous modeling approach is to assume that the membrane can swell freely (for examples, see Weber and Newman,[3] Meyers and Newman,[7] and Springer et al.[8]). This treatment ignores the physical situation wherein the membrane is constrained by the other layers in the fuel-cell sandwich. Finally, swelling has been addressed by some microscopic models (for examples, see Eisenberg,[9] Mauritz and Rogers,[10] Datye et al.,[11] Din and

Correspondence concerning this article should be addressed to A. Z. Weber at aweber@newman.cchem.berkeley.edu.

Michaelides,[12] Paddison,[13] and Eikerling et al. [14,15]), but such models are too unwieldy to use in an overall fuel-cell model, although they do provide some of the basis for the physical arguments in this article. Furthermore, such models examine only local effects (such as within single clusters, molecular sites, or pores). This article explicitly accounts for swelling and the stress associated with constraint in a macrohomogeneous model.

The outline of the article is as follows. Because our previous PEM model forms the basis of this report, it is summarized first. Second, the physical effects of constraining the membrane are presented, followed by the mathematical treatment. Results and discussion are then presented, including the examination of the magnitude and general effects of constrained membranes and one-dimensional (1-D) simulation results on water management. Finally, overall conclusions and remarks are made.

Review of membrane model

In previous papers, we presented both a physical and a mathematical model of PEMs that described many effects not incorporated into current models.[3,16] Because the addition of the stress relations is directly tied to the PEM model, it is reviewed here. The main variable of the model is the water content of the membrane λ (moles of water per mole of sulfonic acid sites).

As discussed thoroughly in a previous paper,[3] concentrated-solution theory is used to derive four governing equations for transport in the membrane system of membrane, protons, and water. These equations contain four unknowns: $\mathbf{\Phi}$, the electrical potential; $\mathbf{i}$, the current density, which is specified; $\mathbf{N}_0$, the superficial flux density of water; and μ_0, the chemical potential of water. The model assumes steady state and isothermal operation. For a three-species system, there are three transport properties. These are identified as κ, the conductivity of the membrane; ξ, the electroosmotic coefficient or number of waters carried per proton in the absence of a concentration gradient; and α, the transport coefficient, defined by

$$\mathbf{N}_0 = -\alpha \nabla \mu_0 \tag{1}$$

All the transport properties are functions of temperature and water content λ. Table 1 summarizes the governing equations, definitions, and transport properties as discussed below. In the first part of the table are some useful definitions and the current and water material balances, Eqs. 1-9 and 1-10, respectively.

There are two transport modes in the membrane. One is associated with a membrane in contact with a vapor reservoir, and the other is associated with a membrane in contact with a liquid reservoir. These two modes are termed the vapor-equilibrated and liquid-equilibrated transport mode, respectively. The two modes are a key component of the membrane model and help both to bridge the gap between current models in the literature and to account for observed phenomena such as Schroeder's paradox: a difference in the membrane water uptake from a liquid reservoir and a saturated-vapor reservoir at the same chemical potential (for a further discussion see Weber and Newman[16]).

In the vapor-equilibrated mode, the membrane is treated as a one-phase system in which water dissolves and moves through clusters and collapsed channels by diffusion. In this transport mode, the governing transport equations for current and water are Eqs. 1-11 and 1-12, respectively. λ_V, the water content in the vapor-equilibrated portion of the membrane, is determined by a modified version of the chemical model of Meyers and Newman[17] that accounts for temperature and stronger binding at low water-vapor activities.[3] The vapor-equilibrated transport mode is dominant when the gas stream does not contain saturated or nearly saturated water vapor. The functional forms and modeling equations for the vapor-equilibrated transport mode are summarized in the second part of Table 1.

In the liquid-equilibrated mode, the membrane is treated as a two-phase system composed of membrane and liquid water. Thus, the membrane is similar to a porous medium through which liquid water moves as a result of convection (that is, a pressure gradient). In this transport mode, the governing transport equations (Eqs. 1-17 and 1-18) are similar to the vapor-equilibrated ones except that the liquid-equilibrated properties are used and the chemical potential of water has been substituted by

$$\nabla \mu_0 = \bar{V}_0 \nabla p_L \tag{2}$$

where the subscript L denotes the liquid phase or liquid-phase property and $\bar{V}_0$ is the (partial) molar volume of water. The water content λ_L is equal to a value of 22. The functional forms and modeling equations for the liquid-equilibrated transport mode are summarized in the third part of Table 1.

When the membrane is neither fully liquid nor vapor equilibrated, transport occurs through both modes, which are assumed to operate in parallel. In this instance, the governing transport equations are assumed to be a superposition of the two transport mode equations, and are averaged by the fraction of expanded channels S (Eqs. 1-23 and 1-24). The value of S is calculated by integrating the channel-size distribution from a critical radius—determined by the liquid pressure and channel properties (Eq. 1-28)—to infinity, given that the channels are hydrophobic. The hydrophobic channels ensure that, when there is no liquid-water reservoir, there is no liquid in the channels and also that vapor expand the collapsed channels. Because both μ_0 and p_L are being used as variables, an additional relation is needed between them, which is given by an equilibrium expression that is the same in form as Eq. 2. The functional forms and modeling equations for the simultaneous occurrence of both transport modes are summarized in the fourth part of Table 1.

Effects of Constraining the Membrane

Physical effects

PEMs normally contain a bound hydrophilic anion, such as a sulfonic group, and as such have a strong affinity toward water and other polar solvents. This affinity causes them to swell.[18-22] From a fundamental perspective, this behavior is relatively straightforward. The uptake of water hydrates the hydrophilic groups, which form clusters and channels that expand. This expansion pushes out the polymer matrix, and thus the overall ionomer system volume increases. For a liquid-equilibrated membrane, the increase in volume is about 74%.[19]

As mentioned above, fuel-cell operation and design do not allow for swelling, and the membrane is at least partially

Table 1. Governing Equations and Modeling Parameters by Transport Mode for the Membrane Model

General definitions and equations

$$\bar{V}_0 = \frac{M_0}{\rho_0} \tag{1-1}$$

$$\bar{V}_m = \frac{EW}{\rho_{m,o}} \tag{1-2}$$

$$V = \bar{V}_m + \lambda \bar{V}_0 \tag{1-3}$$

$$f = \frac{\lambda \bar{V}_0}{V} \tag{1-4}$$

$$\rho = \frac{EW + M_0 \lambda}{V} \tag{1-5}$$

$$c_0 = \frac{\lambda}{\bar{V}} \tag{1-6}$$

$$x_0 = \frac{\lambda}{\lambda + 1} \tag{1-7}$$

$$l = l_o\left(1 + 0.36\,\frac{\hat{\lambda}\bar{V}_0}{\bar{V}_m}\right) \tag{1-8}$$

$$\nabla \cdot \mathbf{i} = 0 \tag{1-9}$$

$$\nabla \cdot \mathbf{N}_0 = 0 \tag{1-10}$$

Vapor-equilibrated transport mode equations and parameters

$$\mathbf{i} = -\kappa_V \nabla\Phi - \frac{\kappa \xi_V}{F}\nabla\mu_0 \tag{1-11}$$

$$\mathbf{N}_0 = -\frac{\kappa_V \xi_V}{F}\nabla\Phi - \left(\alpha_V + \frac{\kappa_V \xi_V^2}{F^2}\right)\nabla\mu_0 \tag{1-12}$$

$\lambda_V = \lambda_V(\mu_0, T)$ from model of Weber and Newman[3]

$$\kappa_V = 0.5(f_V - 0.06)^{1.5}\exp\left[\frac{15{,}000}{R}\left(\frac{1}{T_{ref}} - \frac{1}{T}\right)\right] \tag{1-13}$$

$\xi_V = \lambda \quad$ for $\lambda < 1$

$$\xi_V = 1 \quad \text{for } \lambda \geq 1 \tag{1-14}$$

$$\alpha_V = \frac{c_{0,V} D_{\mu_0}}{RT(1 - x_{0,V})} \tag{1-15}$$

$$D_{\mu_0} = 1.8 \times 10^{-5} f_V \exp\left[\frac{20{,}000}{R}\left(\frac{1}{T_{ref}} - \frac{1}{T}\right)\right] \tag{1-16}$$

Liquid-equilibrated transport mode equations and parameters

$$\mathbf{i} = -\kappa_L \nabla\Phi - \frac{\kappa \xi_L}{F}\bar{V}_0 \nabla p_L \tag{1-17}$$

$$\mathbf{N}_0 = -\frac{\kappa_L \xi_L}{F}\nabla\Phi - \left(\alpha_L + \frac{\kappa_L \xi_L^2}{F^2}\right)\bar{V}_0 \nabla p_L \tag{1-18}$$

$$\lambda_L = 22 \tag{1-19}$$

$$\kappa_L = 0.5(f_L - 0.06)^{1.5}\exp\left[\frac{15{,}000}{R}\left(\frac{1}{T_{ref}} - \frac{1}{T}\right)\right] \qquad \text{for } f \leq 0.45$$

$$\kappa_L = \kappa_L(0.45, T) \qquad \text{for } f \geq 0.45 \tag{1-20}$$

$$\xi_L = 2.55\,\exp\left[\frac{4000}{R}\left(\frac{1}{T_{ref}} - \frac{1}{T}\right)\right] \tag{1-21}$$

$$\alpha_L = \frac{k_{sat}}{\mu \bar{V}_0^2}\left(\frac{f}{f_L}\right)^2 \tag{1-22}$$

Both transport modes equations and parameters

$$\mathbf{i} = S\left(-\kappa_L \nabla\Phi - \frac{\kappa_L \alpha_L}{F}\bar{V}_0 \nabla p_L\right) + (1 - S)\left(-\kappa_V \nabla\Phi - \frac{\kappa_V \xi_V}{F}\nabla\mu_0\right) \tag{1-23}$$

$$\mathbf{N}_0 = S\left[-\frac{\kappa_L \xi_L}{F}\nabla\Phi - \left(\alpha_L + \frac{\kappa_L \xi_L^2}{F^2}\right)\bar{V}_0 \nabla p_L\right] + (1 - S)\left[-\frac{\kappa_V \xi_V}{F}\nabla\Phi - \left(\alpha_V + \frac{\kappa_V \xi_V^2}{F^2}\right)\nabla\mu_0\right] \tag{1-24}$$

$$\nabla\mu_0|_V = \bar{V}_0 \nabla p_L|_L \tag{1-25}$$

$$\lambda = \lambda_V|_{a_0 = 1} + (\lambda_L - \lambda_V|_{a_0 = 1})S \tag{1-26}$$

$$S = \frac{1}{2}\left\{1 - \text{erf}\left[\frac{\ln r_c - \ln(1.25)}{0.3\sqrt{2}}\right]\right\} \tag{1-27}$$

$$r_c = -\frac{2\gamma \cos\theta}{p_L} \tag{1-28}$$

constrained. Physically, a constrained membrane has a lower value of λ than that of a swollen one. The physical picture being described is that of a sponge between two spring-loaded meshes. Thus, if the applied pressure is high enough, it compresses the membrane, which results in a loss of water. Another way to think of this is that, by conservation of the overall membrane-matrix mass, a smaller total volume means that some of the water must be pushed out.

The ionic clusters that form in the membrane are attributed to equilibrium between electrostatic forces and the deformation energy of the polymer. A constrained membrane has a higher deformation energy, and thus the clusters should be slightly smaller, much like the case of higher equivalent weight membranes. However, the number of sulfonic acid sites has to remain constant. Thus, although the energy to deform the polymer is higher, so also is the number of sulfonic acid sites for a given volume, and thus the electrostatic energy also increases. The resultant picture for a constrained membrane is a cluster-network model in which the clusters are only slightly smaller, but are pushed closer together. Furthermore, it is assumed that the channel-size distribution (that is, the diameter of the channel) remains the same. The argument is the same as that presented previously,[3] and is similar to the cluster discussion above wherein the extra forces all increase. Thus, the trade-offs between them are the same, especially for the very thin channels within the flexible ionomer backbone.

From the above picture, one can envision that the water volume fraction might be higher for a constrained vs. an unconstrained membrane placed in the same water reservoir. This is because, even though the constrained membrane has a lower water content λ, its overall volume is also smaller, and thus its water volume fraction may be higher (see Eq. 1-4). If this occurs, then the transport properties of the medium such as the conductivity will be unchanged or may even increase upon constraint. Thus, property values and dependencies should be experimentally measured for membranes constrained to their expected dimensions under operation. Such measurements are not really available in the literature. Finally, although the above example is for conductivity, the transport coefficients could also be affected in the same manner; however, the electroosmotic coefficients should remain unchanged. Finally, because a constrained membrane has a smaller thickness than that of an unconstrained one, the various gradients are larger and this couples with any change in the transport properties to determine the superficial fluxes. This last point is discussed in terms of the simulation results below.

Mathematical model

Swelling studies of the membrane have shown that the assumption of additive molar volumes is valid.[19,22] By this assumption, the volume of a free-swelling membrane in terms of water content is given by

$$V_f = V_o\left(1 + \frac{\hat{\lambda}_f \bar{V}_0}{\bar{V}_m}\right) \tag{3}$$

where the subscript f denotes the case of a free-swelling membrane, V_o is the initial volume of the dry membrane, $\hat{\lambda}_f$ is the average value of λ in the free-swelling membrane, and $\bar{V}_m$ is the partial molar volume of the membrane. Because $\hat{\lambda}_f$ is an unknown quantity initially, a scheme must be used to obtain the final membrane volume (or in 1-D simulations, the membrane thickness; see Eq. 1-8). The scheme used is to iterate the simulations successively until the value of $\hat{\lambda}_f$ converges, as we discussed in a previous report.[3]

A membrane operating in a fuel cell might not be fully constrained. In this situation, a degree-of-constraint parameter should be used. This parameter dictates how constrained the membrane is with respect to its free-swelling state. Using this parameter, Eq. 3 becomes

$$V_{con} = V_o\left[1 + \frac{\hat{\lambda}_f \bar{V}_0}{\bar{V}_m}(1 - \chi)\right] \tag{4}$$

where the subscript *con* denotes a constrained membrane and χ is the degree of constraint (1 for a fully constrained membrane and 0 for a free-swelling membrane). This new volume should be used in the relevant expressions in Table 1 such as water volume fraction and density, Eqs. 1-4 and 1-5, respectively. For understanding purposes, a definition of χ can be written by combining Eqs. 3 and 4 and solving for χ

$$\chi = \frac{V_f - V_{con}}{V_f - V_o} \tag{5}$$

Thus, χ is a volume ratio that can be experimentally realized by either compressing a swollen membrane to a specified volume or by applying a pressure and determining the volume change for a given set of conditions.

To account for the effect of stress on the constrained membrane and how it alters the membrane's water content, a relatively straightforward approach is used. It is similar to that done in the literature to determine cluster size and elasticity.[23,24] The approach is shown schematically in Figure 1 for the case of a fully constrained membrane, where τ is the dilatation stress. Three different membrane states are identified. State 1 is the dry, initial membrane; state 2 is the free-swelling membrane where it has been placed in a water reservoir of chemical potential μ_0^{ext}; and state 3 is the fully constrained membrane in the same water reservoir. From the figure, one can visualize the physical picture and the definition of χ. Whereas $\hat{\lambda}_f$ is calculated by our previous model, the stress and water content must be determined for the constrained membrane, state 3.

For an equilibrated membrane, the chemical potential of the water in the reservoir and that just inside the membrane are equal, whether the membrane is constrained or swollen, as shown in Figure 1. Like the sponge analogy, compression of the membrane by the other fuel-cell layers does not directly affect the water because the stress represents an external body force that is felt by the membrane matrix only, as discussed elsewhere.[3,25] Mathematically, this equilibrium can be expressed as

$$\mu_0^{(2)} = \mu_0^{ext} = \mu_0^{(3)} \tag{6}$$

where the numbers refer to membrane states 2 and 3 in Figure 1. Using the thermodynamic development of Meyers and New-

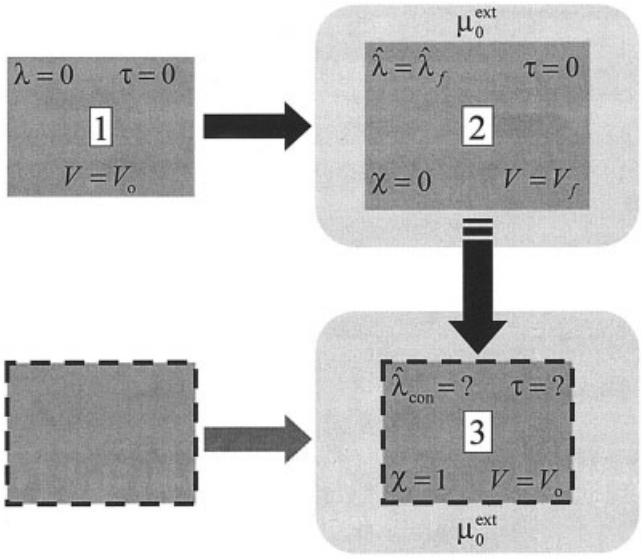

Figure 1. Schematic showing the modeling approach going from the initial, dry membrane (1) to the free-swelling membrane (2) to the constrained membrane (3), which in this case is fully constrained.

The gray boxes are the different membrane states, the dashed line is the membrane constraint attributed to the other fuel-cell sandwich layers, and the light gray is the water reservoir.

man,[17] expressions can be written for the chemical potential of water in the two membranes, as follows:

$$\mu_0^2 = \mu_0^* + RT \ln \hat{\lambda}_f EW + 2RT \sum_{k=1}^{n} E_{0,k}^* m_k$$

$$\mu_0^3 = \mu_0^* + RT \ln \hat{\lambda}_{con} EW + 2RT \sum_{k=1}^{n} E_{0,k}^* m_k + \bar{V}_0 \tau \quad (7)$$

where μ_0^* is a combination of reference states and constants, m_k is the molality of species k in the membrane, $E_{0,k}^*$ represents the binary interaction parameter between water and species k. The summation is over the total number of species n, in the membrane (such as protons); EW is the equivalent weight of the membrane, and the molality of water in the membrane has been replaced by the product $\hat{\lambda}EW$. The above relationships use average values of the water content because it is assumed that the stress acts more-or-less uniformly on the membrane (for a further discussion, see the dissertation by Meyers[26]).

Next, we assume that the binary interaction parameters are constant, which is not necessarily true because of such phenomena as heats of solvation, but is a very good first approximation. Also, the molalities of the other species are assumed to be constant, which is a valid first approximation because of electroneutrality and the regime in which swelling, and thus constraint, is important (that is, at high water contents). These assumptions, along with Eqs. 6 and 7, allow for an expression to be written detailing how the chemical potential of water changes when going from the swollen to the constrained membrane, states 2 and 3, respectively:

$$\Delta\mu_0 = RT\Delta \ln \hat{\lambda} + \bar{V}_0 \tau = 0 \quad (8)$$

Solving the above equation for the change in the average water content of the membrane yields

$$\frac{\hat{\lambda}_{con}}{\hat{\lambda}_f} = \exp\left(-\frac{\bar{V}_0 \tau}{RT}\right) \quad (9)$$

Although Eq. 9 represents the governing equation, a relation is still needed for τ. The dilatation stress of going from the free-swelling to the constrained state can be expressed as

$$\tau = \frac{d}{dV}\left(\frac{K}{V}\right) = -K \ln\left(\frac{V_{con}}{V_f}\right) \quad (10)$$

where K is the bulk modulus of the membrane/water system. This modulus has been derived both experimentally and theoretically for Nafion[27-29] and can be expressed as

$$K = \frac{Y}{3} = \frac{275}{3}\left(\frac{T_{ref}}{T}\right)\exp\left[-0.1655\left(\frac{\hat{\lambda}M_0}{EW} + \frac{1200 - EW}{100}\right)\right] \quad (11)$$

where Y is Young's modulus and M_0 is the molecular weight of water. The above form takes into account the plasticizing effect of water on the membrane, although a different dependency on water content has recently been observed.[30] The temperature dependency is derived from the data of Yeo and Eisenberg[31] and Escoubes et al.[1] and has an expected inverse relationship. It should be noted that this expression is valid only in the temperature range below the glass-transition temperature. As the glass-transition temperature is approached, the modulus will vary more significantly, and an adjustment will have to be made to Eq. 11.

Finally, Eqs. 3, 4, 9, and 10 can be combined and simplified to yield a single governing equation

$$\frac{\hat{\lambda}_{con}}{\hat{\lambda}_f} = \left[\frac{\bar{V}_m + \bar{V}_0(1-\chi)\hat{\lambda}_f}{\bar{V}_m + \bar{V}_0\hat{\lambda}_f}\right]^{K\bar{V}_0/RT} \quad (12)$$

where Eq. 11 is used to calculate the bulk modulus. An average value for K should be used, and this makes the above equation implicit. However, if Eq. 11 is used, the deviation is normally less than 5% with the change in water content.

The way in which the above equations and approach are used in a simulation is as shown in Figure 1. Simulations are done in which the membrane can freely swell, and a value of $\hat{\lambda}_f$ is calculated. Next, the constrained volume is set by fixing a value of χ, or by doing a stress balance. Equation 12 is then used to calculate the change in the value of $\hat{\lambda}$. Finally, this ratio is used with the constrained volume, V_{con}, in another simulation. The ratio modifies the value of λ, determined by the membrane model, at each mesh point.

Results and Discussion

The results and discussion are divided into three parts. In the first part, general effects of constraint are discussed, including changes in the transport-property and water-uptake values with respect to the degree of constraint. In the second part, some 1-D simulation results are investigated with respect to fuel-cell water management. Finally, the magnitude of the stress and the existence of constrained membranes are discussed. Unless noted, all of the analyses below assume a Nafion membrane with an equivalent weight *EW* of 1100 g/equiv and a dry density $\rho_{m,o}$ of 2 g/cm^3.

General effects of constraint

Constraining the membrane primarily affects is water content and volume. The differences in the value of λ for free-swelling and fully constrained membranes at a given water-vapor activity is shown in Figure 2. The uptake curves show that the effect of constraint is more pronounced at higher water-vapor activities. Figure 2 also demonstrates that constraint is more significant for liquid-equilibrated vs. vapor-equilibrated membranes. These results make physical sense because the membrane swells more at the higher values. The value of λ for a constrained saturated-vapor-equilibrated membrane ($a_0 = 1$) is in agreement with experimental findings,[1] and there is a nearly 20% reduction in λ at 30°C.

It is known that λ for vapor-equilibrated membranes is temperature dependent below the glass-transition temperature,[3,32-34] with λ decreasing with increasing temperature at a given water-vapor activity. Figure 3 shows the effect of temperature on λ for a saturated-vapor-equilibrated membrane that can freely swell or is fully constrained. The figure shows that an increase in temperature causes a lower value of λ as well as a lesser effect of constraint (about half the reduction in λ at 80°C than at 30°C). The latter is attributed to the lower value of the bulk modulus with temperature, and the inverse temperature dependence of the exponent in Eq. 12. Both Figures 2 and 3 demonstrate that constraining the membrane can have a significant effect on its water uptake. They also emphasize that water uptake should be measured in conditions similar to those in operation, and may explain some of the variability in comparing isotherms and uptake values from different sources.

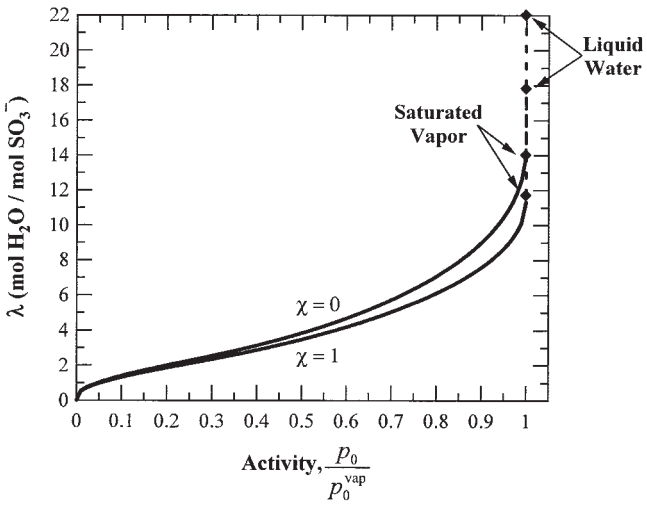

Figure 2. Water uptake isotherms for a fully constrained ($\chi = 1$) and a free-swelling ($\chi = 0$) membrane at 30°C.

The dotted line shows the effect of Schroeder's paradox.

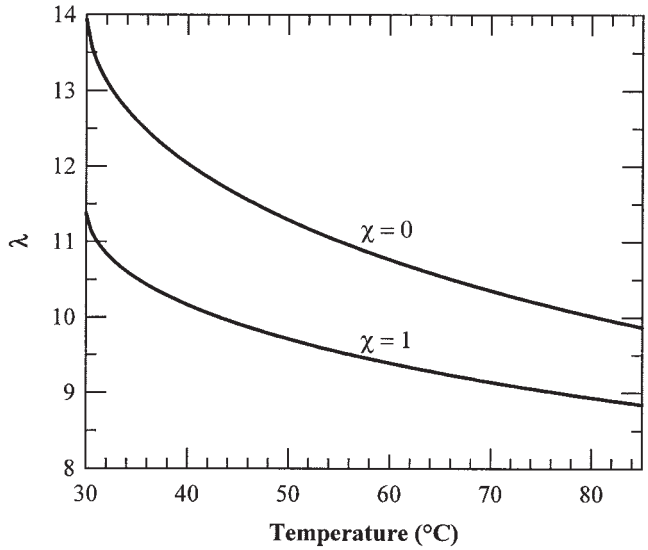

Figure 3. Water content of a saturated-vapor-equilibrated membrane as a function of temperature for both a fully constrained ($\chi = 1$) and a free-swelling ($\chi = 0$) membrane.

Because the transport properties are functions of the water content, they will change because of constraint. Only the electroosmotic and liquid-equilibrated transport coefficients are not expected to vary significantly because they are not strong functions of the water content (see Eqs. 1-14, 1-21, and 1-22). As seen in Table 1, the other transport properties are direct functions of the water content λ or the water volume fraction *f*. Although the water content decreases with constraint, the water volume fraction may increase as a result of the lower total volume of the membrane system. Thus, if the formulas from Table 1 are used, the properties may actually increase upon constraint, as shown in Figure 4 for the conductivity and transport coefficient (see Eqs. 1-13 and 1-15, respectively) of a saturated-vapor-equilibrated membrane. Figure 4 also shows that if the properties are assumed to be functions of λ instead of *f*, then their values decrease with constraint. It should be noted that both properties should change in the same fashion because of their similar underlying physical phenomena. Herein it is assumed that the properties are functions of *f* (that is, as written in Table 1) because the formula for conductivity is well known and accepted.[3] The above results demonstrate that changes in transport-property values can be significant because of constraint. In addition, changes in the property expressions besides those resulting from water content and volume have not been considered. Therefore, transport-property data should be taken in conditions that mimic the fuel-cell operating conditions. For example, because transport-property data are often measured with a free-swelling membrane, they are not necessarily representative of those during operation.

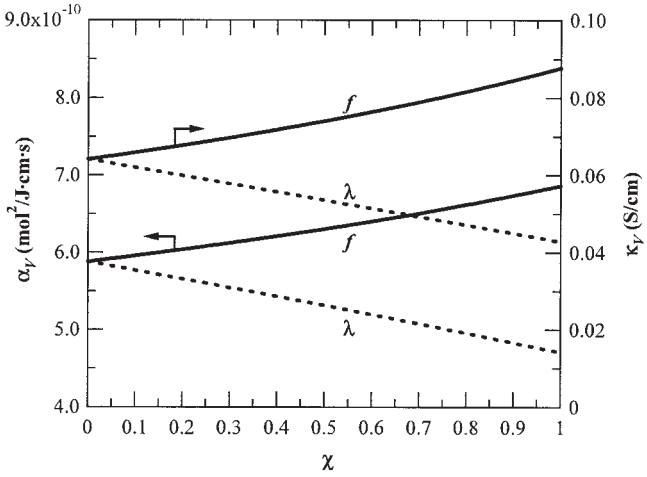

Figure 4. Conductivity and transport coefficient as a function of degree of constraint for a saturated-vapor-equilibrated membrane at 30°C.

The two sets of lines represent whether the conductivity and diffusion coefficient are taken to be direct functions of λ (dotted) or f (solid).

Effects of constraint on water management

It is well known that an understanding of water management is crucial in the operation and design of fuel cells. To examine the effect of constraint on water management, some simple 1-D fuel-cell sandwich simulations were run. The simulations use the simple sandwich model that has been described elsewhere.[35] The modeling domain consists of the membrane, two diffusion media, and two gas channels. The membrane is treated with the equations from Table 1 with the above stress equations and methodology. The diffusion media are treated with Stefan–Maxwell diffusion for the gas phase and Darcy's law for the liquid phase, and the gas channels are assumed to be perfectly mixed. Figure 5 shows the modeling domain and the relevant modeling equations. Because only the water balance is being studied, the catalyst layers can be assumed to be infinitely thin, and the production of water and consumption of reactants to be given by Faraday's law at the specified current density.

To use the model, boundary conditions, simulation parameters, and property values are necessary. The boundary conditions have been discussed previously[35] and are summarized in Table 2. The values for the properties and the simulation conditions not already given are in Table 3, and the membrane is assumed to be pinched or, in other words, constrained on all sides. The effect of constraint on the water balance is analyzed in terms of the parameter β, the net flux of water in the membrane per proton flux

$$\beta = \frac{\mathbf{N}_0}{\mathbf{i}/F} \tag{13}$$

A positive value of β signifies that the net movement of water in the membrane is from anode to cathode.

The first simulations presented use saturated hydrogen and air and break down the effect of constraint into its components, as shown in Figure 6. Figure 6a demonstrates that the net flux of water in the membrane is affected by constraint. In fact, fully constraining the membrane causes it to decrease by about a factor of 4. This is important because the lower the value of β, the lower the effect of flooding, given that water is produced at the cathode. From strictly a water-management perspective, constraining the membrane is beneficial, at least with saturated-gas feeds. The net flux of water in the membrane is a composite of the back flux attributed to the water chemical-potential gradient and the electroosmotic flux. Because the electroosmotic flux is relatively independent of the degree of constraint (the current density remains constant and the electroosmotic coefficient for each membrane type is assumed independent of stress effects), the reason that β decreases must be attributed to the increase in the back flux of water from cathode to anode, as shown in the solid line of Figure 6b.

Simulations allow for an in-depth look and breakdown of the dominant phenomena that occur. Thus, one can run simulations under conditions that are impossible to do experimentally. In Figure 6b, two separate simulation cases were run. The first case is that λ changes attributed to constraint, but the volume does not (that is, $V_{con} = V_f$). The second case is the opposite; that is, that the volume changes because of constraint but the value of λ remains constant (that is, $\hat{\lambda}_{con} = \hat{\lambda}_f$ but $V_{con} \neq V_f$). It is clear from the figure that the increase in the back flux is mainly a result of the decrease in the membrane volume or thickness. This decrease directly exerts an impact on the flux by increasing the gradient of water chemical potential in the membrane. In addition, according to our assumption, the transport properties increase because of the higher water volume fraction. Similarly, although the electroosmotic flux is constant at the assumed current density, the potential drop through the membrane decreases with constraint because of the membrane's smaller thickness. However, this decrease also depends on whether the conductivity increases or decreases upon constraint. When the volume is held constant, the back flux of water decreases because the lower value of λ causes a lower water volume fraction, and thus lower transport-property values. This is a different case from that in Figure 4 because the volume is not changing (that is, f decreases instead of increases). Overall, the effect of constraint on the water balance is significant and is dominated by the membrane's smaller volume, which causes a higher back flux of water from cathode to anode.

The results in Figure 6a are valid for saturated feeds where the liquid-equilibrated transport mode is dominant. To deter-

*a*GC	Diffusion Medium	Membrane	Diffusion Medium	*c*GC
	$\nabla p_0 = \frac{RT}{pD^{\text{eff}}_{H_2}}\left(p_0\frac{\mathbf{i}}{2F} - (p_a - p_0)\mathbf{N}_0^G\right)$		$\nabla p_0 = \frac{RT}{pD^{\text{eff}}_{O_2}}\left(-p_0\frac{\mathbf{i}}{4F} - (p_c - p_0)\mathbf{N}_0^G\right)$	
	$\mathbf{N}_0^L = -\alpha_L^L \bar{V}_0 \nabla p_L$	see Table 1	$\mathbf{N}_0^L = -\alpha_L^L \bar{V}_0 \nabla p_L$	
	$\nabla \cdot \mathbf{N}_0^G = \frac{k_{\text{evap}}}{RT}\left(p_0^{\text{vap}} - p_0\right)$		$\nabla \cdot \mathbf{N}_0^G = \frac{k_{\text{evap}}}{RT}\left(p_0^{\text{vap}} - p_0\right)$	
	$\nabla \cdot \mathbf{N}_0^L = -\frac{k_{\text{evap}}}{RT}\left(p_0^{\text{vap}} - p_0\right)$		$\nabla \cdot \mathbf{N}_0^L = -\frac{k_{\text{evap}}}{RT}\left(p_0^{\text{vap}} - p_0\right)$	

$z \longrightarrow$

Figure 5. 1-D modeling sandwich and governing equations.

Table 2. Boundary Conditions by Region and Variable for the 1-D Sandwich Model Including the Different Transport Modes

Region of Operation	Variable	Interface	Boundary Condition
		Always valid	
aDM	$p_{0,a}$	aGC/aDM	$p_{0,a} = p_{0,a}$ from activity
cDM	$p_{0,c}$	cDM/cGC	$p_{0,c} = p_{0,c}$ from activity
aDM	p_L	aGC/aDM	$p_L = p_a$
cDM	p_L	cDM/cGC	$p_L = p_c$
All	$\mathbf{i}$	aGC/aDM	$\mathbf{i}$ = specified
Mem.	$\mathbf{N}_0$	aDM/Mem.	$\mathbf{N}_0 = \mathbf{N}_0^G + \mathbf{N}_0^L$
Mem.	$\mathbf{\Phi}$	Mem./cDM	$\mathbf{\Phi} = 0$
		Liquid and vapor boundary	
Mem.	p_L	Mem./cDM	$\mathbf{N}_0 + \frac{\mathbf{i}}{2F} = \mathbf{N}_0^G + \mathbf{N}_0^L$
Mem.	μ_0	Mem./cDMμ	$\mu_0 = \bar{V}_0(p_c - 0.1)$
aDM	$\mathbf{N}_{0,a}^G$	aDM/Mem.	$p_{0,a} = p_0^{vap}$
cDM	$\mathbf{N}_{0,c}^G$	Mem./cDM	$p_{0,c} = p_0^{vap}$
aDM	$\mathbf{N}_{0,a}^L$	aDM/Mem.	$p_L = p_L$
cDM	$\mathbf{N}_{0,c}^L$	Mem./cDM	$p_L = p_L$
		Only vapor boundary	
Mem.	p_L	Mem./cDM	$p_L = 0$
Mem.	μ_0	Mem./cDM	$\mathbf{N}_0 + \frac{\mathbf{i}}{2F} = \mathbf{N}_0^G + \mathbf{N}_0^L$
aDM	$\mathbf{N}_{0,a}^G$	aDM/Mem.	$\mu_0 = RT\ln\left(\frac{p_{0,a}}{p_0^{vap}}\right) + \bar{V}_0(p_a - 0.1)$
cDM	$\mathbf{N}_{0,c}^G$	Mem./cDM	$\mu_0 = RT\ln\left(\frac{p_{0,a}}{p_0^{vap}}\right) + \bar{V}_0(p_a - 0.1)$
aDM	$\mathbf{N}_{0,a}^L$	aDM/Mem.	$\mathbf{N}_{0,a}^L = 0$
cDM	$\mathbf{N}_{0,c}^L$	Mem./cDM	$\mathbf{N}_{0,c}^L = 0$

mine whether the results are general, simulations were run where the humidity of the gases in the gas channels was varied. The results of these simulations are given in Figure 7. It is clear that the effect seen in Figure 6a is valid in general: constraining the membrane causes a more negative net water flux in the membrane. Of course, this is subject to the property-value expressions used in Table 1, but because the dominant factor upon constraint is the membrane's smaller volume, the trend should remain.

Figure 7 also demonstrates that saturated gases greatly increase the effect of constraint. This result is explained by two reasons. First, the liquid-equilibrated transport coefficient (Eq. 1-22) is much larger than the vapor-equilibrated transport coefficient (Eq. 1-15). Thus, upon constraint, the back flux is much larger. However, the electroosmotic flux is also larger for

Table 3. Values for the Parameters Used in the Simulations

Parameter	Value
	Operating conditions
Membrane	Nafion 115
T	80°C
$\mathbf{i}$	0.4 A/cm^2
p_a	0.15 MPa
p_c	0.15 MPa
	*Modeling properties**
l_{DM}	0.25 cm
$pD_{\mathrm{H_2},0}^{eff}$	0.01098 MPa · cm^2/s
$pD_{\mathrm{N_2},0}^{eff}$	0.00223 MPa · cm^2/s
μ	3.655×10^{-4} Pa · s
ρ_0	0.9707 g/cm^3
γ	0.06258 N/m
p_0^{vap}	0.04732 MPa
k_{evap}	1 l/s
T_{ref}	303.15 K
α_L^L	8.1×10^{-9} mol^2/J · s · cm
θ	90.02°
k_{sat}	4.7×10^{-15} cm^2

*All value references can be found in Weber and Newman.[3]

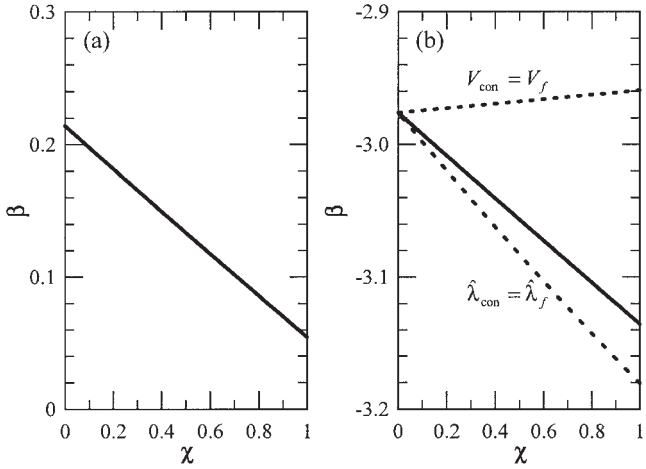

Figure 6. Simulation results of the flux of water in the membrane per proton flux as a function of degree of constraint for saturated feeds and the conditions in Table 4.

(a) Value of the net flux of water in the membrane per proton flux. (b) Solid line is the back flux of water in the membrane per proton flux resulting from the water chemical-potential gradient; dotted lines represent simulations in which $\hat{\lambda}_{con} = \hat{\lambda}_f$ or $V_{con} = V_f$ but the other changes are attributed to constraint.

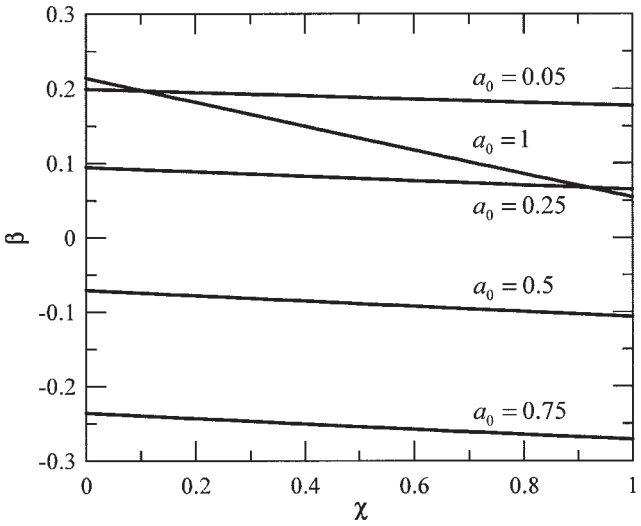

Figure 7. Simulation results of the net flux of water in the membrane per proton flux as a function of degree of constraint and water-vapor activity of air and hydrogen.

the liquid-equilibrated transport mode because of its higher electroosmotic coefficient. The second and more important reason is that, as shown in Figure 2, the lower the water-vapor activity, the lower the value of λ, and thus the lower amount of swelling. This smaller amount means that there is not as great a difference between the swollen and constrained volumes; the effect of constraint is diminished. This explains why constraint has a more significant effect for the saturated-feed case because λ is at least double the value of the other cases as a consequence of Schroeder's paradox.

Figure 7 shows that, as the gases become dry, not only is the effect of constraint lessened, but the water flux from anode to cathode increases after an initial drop from the saturated-gas case. The reason for the decrease is that the liquid-equilibrated transport mode is no longer dominant for the subsaturated-feed cases. This results in a smaller electroosmotic flux, and, due to the faster diffusion of water vapor in hydrogen than air , a larger back flux[35]. Figure 7 suggests that the water balance can be somewhat controlled by the humidity of the feed gases. For example, if the gases in the channels are only slightly humidified, the net water flux in the membrane is negative. A good water-management scheme may be able to hold β close to zero. The unsaturated gas results are strictly valid only when the water vapor in the gas channels is at the prescribed water-vapor activity. They are not necessarily valid when the feed gases are fed at the prescribed humidity because 2-D channel effects (such as the increase in water-vapor activity arising from water production) are ignored. However, the general trends should remain the same, with differences only in quantitative detail. Furthermore, although the simulations are valid for a specific set of conditions, the overall trends and conclusions are the same for different operating conditions including temperature and current density (data not shown). Finally, the results also underline the fact that just swelling of the membrane as a function of water content causes changes in the water balance, and thus it should be included in any fuel-cell model.

Magnitude of constraint and discussion

Although all of the above analysis shows the effects of constraint, the question as to whether a membrane is actually constrained in an operating fuel cell and to what degree has not been answered. To do this, the magnitude of the stress is required. Figure 8 gives the stress as a function of degree of constraint and water-vapor activity. For a fully constrained fully vapor-equilibrated membrane, the stress is 28 MPa at 30°C (33 MPa for a liquid-equilibrated membrane), in agreement with the literature.[1,23,24] As the temperature is increased to 80°C, the stress decreases to 18 MPa for a fully vapor equilibrated membrane (24 MPa for a liquid-equilibrated membrane), in agreement with the trend in Figure 3. Both of the above stresses are substantial, and thus one might not expect a membrane to be fully constrained.

To determine the degree of constraint, the appropriate curve in Figure 8 can be compared to stress–strain relationships for the other materials in the fuel-cell sandwich. A simple analysis involves assuming that the expansion of the membrane compresses only the diffusion media. This is valid because they are the most compressible materials in the sandwich and the catalyst layers are thin enough to be ignored. Now, one can either assume expansion of the membrane in all directions with only a slight anisotropy, the same as in Eq. 1-8 for thickness,[3,18,19,21] or that the edges of the membrane are pinched and thus the diffusion media feel the total amount of stress. In either case, using a stress–strain curve of Toray TGPH-060 paper,[36] allows for the prediction of the stress, diffusion media compression, and degree of membrane constraint. The results of such an analysis are presented in Table 4 for Nafion 112 and 117 at different temperatures and water activities.

For the results in Table 4, the diffusion media were taken to be 300 μm in thickness unstressed and compressed to 250 μm upon fuel-cell assembly. The results clearly show that for all cases the membrane is constrained to a certain extent, although it is less than 50%. Furthermore, only the cases of a liquid-

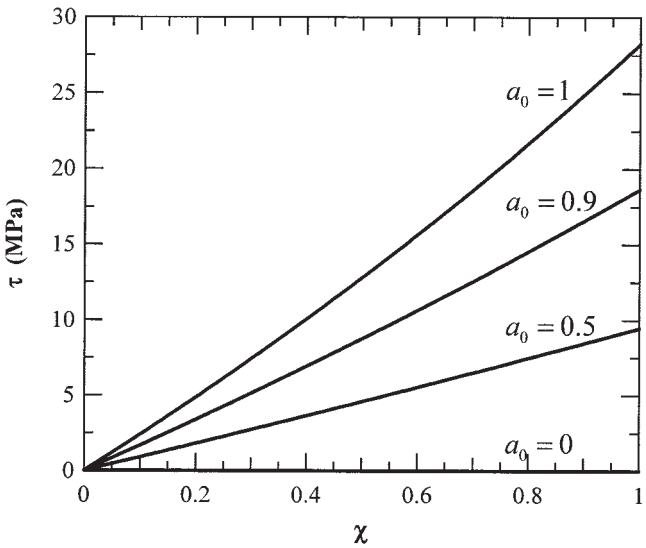

Figure 8. Dilatation stress as a function of degree of constraint for a vapor-equilibrated membrane at 30°C and four different water-vapor activities.

Table 4. Results of Stress Balances for Nafion 117 and 112 Membranes under Different Operating Conditions and Assembled with Toray TGPH-060 Paper Diffusion Media

			Nafion 115			Nafion 112		
a_0*	Pinched**	T (°C)	l_{DM}§ (μm)	χ	τ (MPa)	l_{DM}§ (μm)	χ	τ (MPa)
L	Yes	30	200	0.22	7.2	234	0.14	4.3
L	Yes	60	201	0.24	7.1	234	0.15	4.3
L	Yes	80	202	0.25	7.0	235	0.16	4.3
L	No	30	230	0.15	4.6	244	0.11	3.4
L	No	60	230	0.16	4.6	244	0.12	3.4
L	No	80	231	0.17	4.6	244	0.13	3.4
1	Yes	30	219	0.23	5.6	240	0.16	3.8
1	Yes	60	227	0.26	4.9	243	0.19	3.6
1	Yes	80	229	0.28	4.7	243	0.21	3.5
1	No	30	238	0.16	4.0	246	0.13	3.2
1	No	60	241	0.20	3.7	247	0.17	3.1
1	No	80	242	0.22	3.7	248	0.19	3.1
0.9	Yes	30	232	0.26	4.5	244	0.20	3.4
0.9	Yes	60	234	0.30	4.3	245	0.23	3.3
0.9	Yes	80	235	0.32	4.2	245	0.25	3.3
0.9	No	30	243	0.21	3.5	248	0.18	3.1
0.9	No	60	244	0.24	3.5	248	0.21	3.1
0.9	No	80	244	0.26	3.4	248	0.23	3.1
0.5	Yes	30	244	0.42	3.4	248	0.37	3.1
0.5	Yes	60	245	0.46	3.4	248	0.42	3.1
0.5	Yes	80	245	0.49	3.4	248	0.45	3.1
0.5	No	30	248	0.38	3.1	249	0.36	3.0
0.5	No	60	248	0.42	3.1	249	0.41	3.0
0.5	No	80	248	0.45	3.1	249	0.44	3.0

* L stands for liquid-equilibrated membrane.
**Yes = membrane edges are constrained, all swelling is in the thickness; No = swells in all dimensions.
§ Thickness of a diffusion medium; assembled thickness is 250 μm.

equilibrated membrane and a pinched 117 fully vapor-equilibrated membrane cause significant compression of the diffusion media. As expected, the much thinner 112 membrane does not have as great an effect on the diffusion media as that of the 117, although it is interesting to note that the membranes are constrained to about the same extent for the same set of conditions. The resultant stresses are similar for most cases and are practical (that is, the bipolar plates and fuel-cell assembly can withstand them). It is interesting that the degree of constraint increases with lower water-vapor activity, but this is attributed to the fact that the free swelling and constrained volumes approach each other as the activity is decreased. The actual membrane in terms of thickness is constrained less, as evidenced by the lower value of the stress. Overall, the results agree with the trends described above, and Table 4 clearly shows that membrane constraint should be considered in fuel-cell modeling and design.

The relatively simple analysis leading to the results in Table 4 can be used to enhance modeling simulations and examine alternative materials. For example, other membrane and diffusion-medium stress–strain relationships can be used to examine the stress and thickness of the various components during fuel-cell operation. This is especially important in light of all of the associated effects in terms of transport and water content, as described above, not to mention changes to the structure of the catalyst layers and diffusion media. In addition, comparisons can be made among different materials and design criteria established for both membranes and diffusion media.

The incorporation of stress in a simulation also allows for possible prediction of fuel-cell failure and problems. For example, cycling either temperature or relative humidity results in worse fuel-cell performance.[37,38] Temperature studies show that the pore-size distribution of the electrodes changed, whereas the membrane conductivity remained about constant.[38] In light of the above discussion and Figures 2, 3, and 8, it is conceivable that stress effects might be an important reason for such failure. Furthermore, accelerated testing showed that mechanical failure of the membrane limits the lifetime of the fuel cell.[39] The formation of pinholes can be modeled using a transient model that includes the stress relationships, as can other failure mechanisms such as delamination of the electrodes resulting from stress and even some sealing problems. The last is true in inlet regions where the membrane may be pinched and consequently under higher stress. A full transient analysis also involves the examination of stress in a dynamic fashion where the water uptake rate becomes important. In fact, because of the much faster water uptake for a liquid- than a vapor-equilibrated membrane,[40,41] the stress response could be different enough to affect performance and yield unanticipated problems during start-up and shutdown.

Finally, stress effects may be important in systems that are nonisothermal. For example, the above analysis neglects any additional heating or cooling attributed to the loss of water or the contraction or expansion of the membrane. These factors should be included, especially when examining transient analysis as well as feeds that are subsaturated, where hot spots can develop in the membrane as a consequence of ohmic heating.[42] Furthermore, they may be important in trying to model local effects such as pinhole formation. Another nonisothermal problem deals with fuel-cell operation in subzero conditions, where

freezing may occur. Because the volume of water changes, freezing may exacerbate the stress changes on the local structure, especially during start-up and shutdown. In all, with more data and a slightly more complicated model (such as incorporation of nonisothermal behavior and a more robust elasticity analysis), lifetime predictions and increased understanding into fuel-cell behavior and durability are possible.

Summary and Conclusions

Both a physical picture and a mathematical description of a membrane that is constrained from swelling have been presented. The modeling equations for incorporating stress and constraint into a macrohomogeneous model have been elucidated from a relatively simple approach, and used along with our previous membrane model to analyze the effects of constraint. In most operating fuel cells, the membrane was shown to be relatively constrained (<50%), resulting in significant changes to the water balance, water content, and transport properties. Therefore, the effect of stress and constraint should not be ignored in fuel-cell design and modeling. Of course, some constraint may be desirable from a contact perspective. Furthermore, the incorporation of stress-related phenomena may also lead to a better understanding of fuel-cell failure mechanisms, especially during temperature or humidity cycling and start-up and shutdown.

Constraining the membrane causes the water content of the membrane to decrease. The deviation becomes less as the temperature is increased and the water-vapor activity decreases. The transport properties may also change because of constraint, but, because the volume is smaller, they may actually increase. Experimental data are needed to verify what the property expressions and values are for constrained membranes or the expected state of the membrane during operation. One-dimensional simulation results demonstrated that constraint increases the back flux of water in the membrane from cathode to anode under all humidity conditions. The reason was shown to be explained by the larger gradients in water chemical potential and liquid pressure caused by having a thinner membrane. However, the presented results are strictly valid only for the property expressions used, although the trends and discussion are general. The results demonstrate the need for more data, especially under typical fuel-cell operating conditions, and also perhaps a more complicated model including nonisothermal, dynamic, and more elasticity effects. Overall, the presented model and physical picture bring to light the importance of considering membrane swelling and/or constraint in a model, something that has largely been ignored.

Acknowledgments

This research has been supported by UTC Fuel Cells, LLC, and by an EPA STAR graduate fellowship (91601301-0).

Notation

a_i = activity or species i
c_i = concentration of species i, mol/cm^3
$D_{i,0}^{eff}$ = effective, corrected for porosity and tortuosity, binary diffusion coefficient between species i and water, cm^2/s
D_{μ_0} = diffusion coefficient of water related to a chemical potential driving force, cm^2/s
$E_{0,k}^*$ = binary interaction parameter between water and species k, g/mol
EW = equivalent weight of the membrane, g/equiv
f = water volume fraction of the membrane
F = Faraday's constant, 96,487 C/equiv
$\mathbf{i}$ = superficial current density, A/cm^2
j_0^{evap} = molar evaporation rate of water per unit volume, mol cm^{-3} s^{-1}
k_{evap} = mass-transfer coefficient or rate constant for evaporation, 1/s
k_{sat} = absolute membrane permeability, cm^2
K = bulk modulus, MPa
l_n = thickness of region n, cm
m_k = molality of species k in the membrane, mol/g
M = molecular weight of water, 18.0152 g/mol
n = number of species in the membrane
$\mathbf{N}_i$ = superficial flux density of species i, mol cm^{-2} s^{-1}
p = total pressure, MPa
p_n = total pressure of region n, MPa
p_0^{vap} = vapor pressure of water, MPa
p_i = partial pressure of species i, MPa
p_L = hydraulic or liquid pressure, MPa
r_c = critical pore radius, nm
R = universal gas constant, 8.3143 J mol^{-1} K^{-1}
S = fraction of channels that are expanded
T = absolute temperature, K
V = volume, cm^3
$\bar{V}_i$ = (partial) molar volume of species i, cm^3/mol
x_i = mole fraction of species i
Y = Young's modulus, MPa

Greek letters

α = transport coefficient, mol^2 J^{-1} cm^{-1} s^{-1}
β = net flux of water in the membrane per proton flux
γ = surface tension, N/m
χ = degree of constraint
θ = contact angle, degrees
κ = conductivity, S/cm
λ = moles of water per mole of sulfonic acid sites (water content)
$\hat{\lambda}$ = average membrane water content
μ = viscosity, Pa·s
μ_i = chemical potential of species i, J/mol
μ_0^* = combination of reference states and constants used in Eq. 7
ρ_i = density of species i, g/cm^3
ξ = electroosmotic coefficient
τ = dilatation stress, MPa
$\mathbf{\Phi}$ = potential, V

Subscripts

0 = water
a = anode
c = cathode
con = constrained
f = free swelling
L = liquid-equilibrated membrane
m = membrane
o = initial or reference value
V = vapor-equilibrated membrane

Superscripts

ext = external water reservoir in Figure 1
G = gas phase
L = liquid phase
(2) = free-swelling membrane, state 2 in Figure 1
(3) = constrained membrane, state 3 in Figure 1

Literature Cited

1. Escoubes M, Pineri M, Robens E. Application of coupled thermal-analysis techniques to thermodynamic studies of water interactions with a compressible ionic polymer matrix. *Thermochimica Acta.* 1984; 82:149-160.

2. Benziger JB, Kevrekidis IG. Polymer electrolyte membrane fuel cell reactors. San Francisco, CA: AIChE Annual Meeting; 2003.
3. Weber AZ, Newman J. Transport in polymer-electrolyte membranes. II. Mathematical model. *Journal of the Electrochemical Society*. 2004; 151:A311-A325.
4. Um S, Wang C-Y, Chen KS. Computational fluid dynamics modeling of proton exchange membrane fuel cells. *Journal of the Electrochemical Society.* 2000;147:4485-4493.
5. Nguyen TV, White RE. A water and heat management model for proton-exchange-membrane fuel-cells. *Journal of the Electrochemical Society.* 1993;140:2178-2186.
6. Bernardi DM, Verbrugge MW. Mathematical model of a gas-diffusion electrode bonded to a polymer electrolyte. *AIChE Journal.* 1991;37: 1151-1163.
7. Meyers JP, Newman J. Simulation of the direct methanol fuel cell—II. Modeling and data analysis of transport and kinetic phenomena. *Journal of the Electrochemical Society.* 2002;149:A718-A728.
8. Springer TE, Zawodzinski TA, Gottesfeld S. Polymer electrolyte fuel cell model. *Journal of the Electrochemical Society.* 1991;138:2334-2342.
9. Eisenberg A. Clustering of ions in organic polymers. A theoretical investigation. *Macromolecules.* 1970;3:147-154.
10. Mauritz KA, Rogers CE. A water sorption isotherm model for ionomer membranes with cluster morphologies. *Macromolecules.* 1985;18:483-491.
11. Datye VK, Taylor PL, Hopfinger AJ. Simple model for clustering and ionic transport in ionomer membranes. *Macromolecules.* 1984;17: 1704-1708.
12. Din XD, Michaelides EE. Transport processes of water and protons through micropores. *AIChE Journal.* 1998;44:35-47.
13. Paddison SJ. The modeling of molecular structure and ion transport in sulfonic acid based ionomer membranes. *Journal of New Materials for Electrochemical Systems.* 2001;4:197-207.
14. Eikerling M, Kornyshev AA, Kuznetsov AM, Ulstrup J, Walbran S. Mechanisms of proton conductance in polymer electrolyte membranes. *Journal of Physical Chemistry B.* 2001;105:3646-3662.
15. Eikerling M, Kornyshev AA, Stimming U. Electrophysical properties of polymer electrolyte membranes: A random network model. *Journal of Physical Chemistry B.* 1997;101:10807-10820.
16. Weber AZ, Newman J. Transport in polymer-electrolyte membranes. I. Physical model. *Journal of the Electrochemical Society.* 2003;150: A1008-A1015.
17. Meyers JP, Newman J. Simulation of the direct methanol fuel cell—I. Thermodynamic framework for a multicomponent membrane. *Journal of the Electrochemical Society.* 2002;149:A710-A717.
18. Gebel G, Aldebert P, Pineri M. Structure and related properties of solution-cast perfluorosulfonated ionomer films. *Macromolecules.* 1997;20:1425.
19. Gebel G, Aldebert P, Pineri M. Swelling study of perfluorosulphonated ionomer membranes. *Polymer.* 1993;34:333-339.
20. Yeo RS. Dual cohesive energy densities of perfluorosulfonic acid (Nafion) membrane. *Polymer.* 1980;21:432-435.
21. Hsu CH, Wan CC. An innovative process for PEMFC electrodes using the expansion of Nafion film. *Journal of Power Sources.* 2003;115: 268-273.
22. Oberbroeckling KJ, Dunwoody DC, Minteer SD, Leddy J. Density of Nafion exchanged with transition metal complexes and tetramethyl ammonium, ferrous, and hydrogen ions: Commercial and recast films. *Analytical Chemistry.* 2002;74:4794-4799.
23. Choi P, Datta R. Sorption in proton-exchange membranes. An explanation of Schroeder's paradox. *Journal of the Electrochemical Society.* 2003;150:E601-E607.
24. Dreyfus B. Thermodynamic properties of a small droplet of water around an ion in a compressible matrix. *Journal of Polymer Science Part B: Polymer Physics.* 1983;21:2337-2347.
25. Pintauro PN, Bennion DN. Mass-transport of electrolytes in membranes. 1. Development of mathematical transport model. *Industrial and Engineering Chemistry Fundamentals.* 1984;23:230-234.
26. Meyers JP. Simulation and analysis of the direct methanol fuel cell. PhD Dissertation. Berkeley, CA: Department of Chemical Engineering, University of California; 1998.
27. Li JY, Nemat-Nasser S. Micromechanical analysis of ionic clustering in nafion perfluorinated membrane. *Mechanics of Materials.* 2000;32: 303-314.
28. Hsu WY, Giri MR, Ikeda RM. Percolation transition and elastic properties of block copolymers. *Macromolecules.* 1982;15:1210-1212.
29. Hsu WY, Gierke TD. Elastic theory for ionic clustering in perfluorinated ionomers. *Macromolecules.* 1982;15:101-105.
30. Benziger JB. Personal communication; Mar. 18, 2004.
31. Yeo SC, Eisenberg A. Physical-properties and supermolecular structure of perfluorinated ion-containing (Nafion) polymers. *Journal of Applied Polymer Science.* 1977;21:875-898.
32. Rieke PC, Vanderborgh NE. Temperature-dependence of water-content and proton conductivity in polyperfluorosulfonic acid membranes. *Journal of Membrane Science.* 1987;32:313-328.
33. Broka K, Ekdunge P. Oxygen and hydrogen permeation properties and water uptake of Nafion® 117 membrane and recast film for pem fuel cell. *Journal of Applied Electrochemistry.* 1997;27:117-123.
34. Hinatsu JT, Mizuhata M, Takenaka H. Water-uptake of perfluorosulfonic acid membranes from liquid water and water-vapor. *Journal of the Electrochemical Society.* 1994;141:1493-1498.
35. Weber AZ, Newman J. Transport in polymer-electrolyte membranes. III. Model validation in a simple fuel-cell model. *Journal of the Electrochemical Society*. 2004;151:A326-A339.
36. Gasteiger HA, Mathias MF. Fundamental research and development challenges in polymer electrolyte fuel cell technology. In: Van Zee JW, Fuller TF, Gottesfeld S, Murthy M, eds. *Proton Conducting Membrane Fuel Cells* (Vol. III). Pennington, NJ: The Electrochemical Society Proceeding Series; 2002.
37. Fowler MW, Mann RF, Amphlett JC, Peppley BA, Roberge PR. Incorporation of voltage degradation into a generalised steady state electrochemical model for a PEM fuel cell. *Journal of Power Sources.* 2002;106:274-283.
38. Cho EA, Ko JJ, Ha HY, Hong SA, Lee KY, Lim TW, Oh IH. Characteristics of the pemfc repetitively brought to temperatures below 0°C. *Journal of the Electrochemical Society.* 2003;150:A1667-A1670.
39. Liu W, Ruth K, Rusch G. Membrane durability in PEM fuel cells. *Journal of New Materials for Electrochemical Systems.* 2001;4:227-231.
40. Zawodzinski TA, Derouin C, Radzinski S, Sherman RJ, Smith VT, Springer TE, Gottesfeld S. Water-uptake by and transport through Nafion® 117 membranes. *Journal of the Electrochemical Society.* 1993;140:1041-1047.
41. Nguyen TV, Vanderborgh N. The rate of isothermal hydration of polyperfluorosulfonic acid membranes. *Journal of Membrane Science.* 1998;143:235-248.
42. Fuller TF, Newman J. Water and thermal management in solid-polymer-electrolyte fuel cells. *Journal of the Electrochemical Society*. 1993;140:1218-1225.

Manuscript received Jan. 27, 2004, and revision received Mar. 27, 2004.